

Ab Initio Investigation on the Effect of Transition Metals Doping and Vacancies in WO_3

M. MANSOURI AND T. MAHMOODI*

Department of Physics, Mashhad Branch, Islamic Azad University, Mashhad, Iran

(Received April 28, 2015; in final form January 6, 2016)

We did a density functional theory spin-polarized calculation based on pseudopotential method on the effect of both vacancy and substitutional impurity in the tungsten tri-oxide lattice. We investigated oxygen and tungsten vacancies and for substitutional dopants we used palladium (Pd), platinum (Pt) and gold (Au) atoms with the formula $\text{A}_x\text{W}_{1-x}\text{O}_3$ and $x = 0.125, 0.25, 0.375, 0.5$. We obtained electronic band structure, density of states and magnetization of defected and doped WO_3 . The results show that in the presence of tungsten vacancy, WO_3 acts as a semiconductor with an indirect band gap while oxygen vacancy induces a metallic behavior for WO_3 . Besides, for Pt and Pd the location of trap states lead to photoexcited hole capturing, which can improve photocurrent but for Au dopant, the trap states occur in the middle of the band gap as active recombination centers. Furthermore, both kind of vacancies and Pt dopant can induce magnetization in all values of x , while Pd and Au are less efficient in inducing magnetization.

DOI: [10.12693/APhysPolA.129.8](https://doi.org/10.12693/APhysPolA.129.8)

PACS: 31.15.A-, 61.72.-y, 71.15.Mb, 71.15.Dx

1. Introduction

In recent years, tungsten tri-oxide (WO_3) has grabbed much attention due to its wide technological applications. It is used in semiconductor gas sensors (SGS), electrochromic devices such as smart windows, high temperature super-conductors (HTSCs), photocatalytic water splitting, solar cells and a variety of other applications. Moreover, the possibility of ion intercalation or deintercalation gives rise to several potential applications in secondary rechargeable batteries [1–5]. Low expense, more thermal stability, non-toxicity, high chemical activity and simple structure are just a few of the main ideal intrinsic properties. The injection of electron or hole can cause changes in the properties of tungsten tri-oxide. In particular, photocatalytic activity and gas-sensing property of WO_3 are modified via doping with transition metals such as palladium (Pd), platinum (Pt) and gold (Au) [6–8]. Indeed, band gap engineering is possible via doping. Several attempts have been reported that verify the improvement of photo-activity of WO_3 by selective doping [9–12]. Furthermore, WO_3 doped by Pt represented high stability and recyclability under the experimental conditions and these productions can be used in the photo-oxidation process in order to destroy organic hazards under sunlight radiation [13]. Very recently it has been reported [14] that doping of WO_3 with Pd atoms below 5% reveals no peaks corresponding to the Pd metallic phase in X-ray diffraction (XRD) patterns. Indeed, the ratio of Pd:W below 4% not only shows significant improvement in sensing response time compared to pure samples, but also increasing this ratio causes that the maximum sensitivity temperature decreases. Experi-

mental researches based on several methods like photoacoustic spectroscopy (PAS) or X-ray absorption near edge structure (XANES) show that pure WO_3 is a semiconductor with direct band gap and has a relatively wide band gap ranges from 2.5 to 3.0 eV [15–17]. Similar to other transition metals, several distortions are possible in pure WO_3 as a function of temperature. The most common and stable phase of pure WO_3 is monoclinic structure with the $P2_1/n$ space group from 17 °C to 330 °C [18]. Therefore we use this structure for our calculation.

To study the effects of transition metal doping on electronic structure and the functionality of WO_3 , we investigated the doping of WO_3 with Pt, Pd and Au atoms that are substituted in place of tungsten (W) atoms with different percent of dopant atoms ($\text{A}_x\text{W}_{1-x}\text{O}_3$). In order to compare the results with pure and defected WO_3 we calculated the electronic structure of these systems in the preliminary stage, and then the effects of doping were obtained. In this paper we have reported and analyzed our results on electronic and band structure (BS), density of states (DOS), projected DOS (PDOS) and magnetization properties (μ_{tot}).

2. Computational details

Spin-polarized density functional theory calculations were performed using the Quantum-Espresso package [19, 20] with the plane wave method to calculate the electronic structure of monoclinic lattice of tungsten tri-oxide (WO_3) in the cases of genuine form, defected form with a tungsten and an oxygen vacancies and doped systems in which one of the dopant atoms (palladium (Pd), platinum (Pt) and gold (Au)) substituted with tungsten atoms. Generalized gradient approximation (GGA), and the Perdew–Burke–Ernzerhof (PBE) functional were used for electron exchange-correlation energy [21, 22]. A kinetic energy cut-off of 30 Ry (≈ 400 eV), was used

*corresponding author; e-mail: mahmoodi@mshdiau.ac.ir

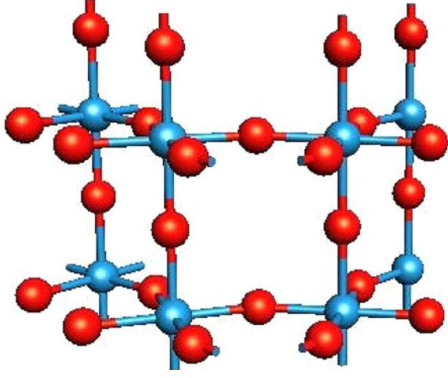


Fig. 1. Schematic view of WO_3 supercell. Blue (O) and red (W).

with a plane-wave basis set. The integration of the Brillouin zone was conducted using a $6 \times 6 \times 6$ Monkhorst–Pack grid with the Γ -point included and a Gaussian broadening with a width of 0.01 eV for smearing was used to guarantee accuracy up to 0.001 Ry. A monoclinic unit cell of $a = 7.30084 \text{ \AA}$, $b = 7.53889 \text{ \AA}$, $c = 7.68962 \text{ \AA}$, $\alpha = 90^\circ$, $\beta = 90.892^\circ$, $\gamma = 90^\circ$ and $V = 53.014 \text{ \AA}^3/\text{cell}$ based on experimental values was used. This structure can be considered as a deformed perovskite ABO_3 struc-

ture, where the A cations are missing, the B cations locate at the center of the octahedron and oxygen atoms are on each unit cell edge midway between the B atoms. This is the same as in the ReO_3 structure. The supercell which was used for all systems is shown in Fig. 1. It consists of 8 tungsten atoms and 24 oxygen atoms and thus is suitable for our desired doping. In each case of calculation all atoms were fully relaxed to obtain geometry optimization and the forces were reduced to 0.02 eV/\AA .

3. Results and discussion

3.1. Bulk

We studied the electronic structure of pure monoclinic WO_3 in the preliminary stage of our study. Our calculation shows that WO_3 in a stoichiometric form is a semiconductor with a direct band gap of 1.89 eV in Γ point which is consistent with previous works [23–25]. It should be mentioned that in comparison with experimental results, the band gap is underestimated as expected for GGA exchange-correlation functional. There is also an indirect band gap in $Z-\Gamma$ which is negligibly ($\approx 0.2 \text{ eV}$) greater than direct band gap. Total and Fermi energies have been obtained of 27.19 Ry/formula unit and 5.09 eV, respectively.

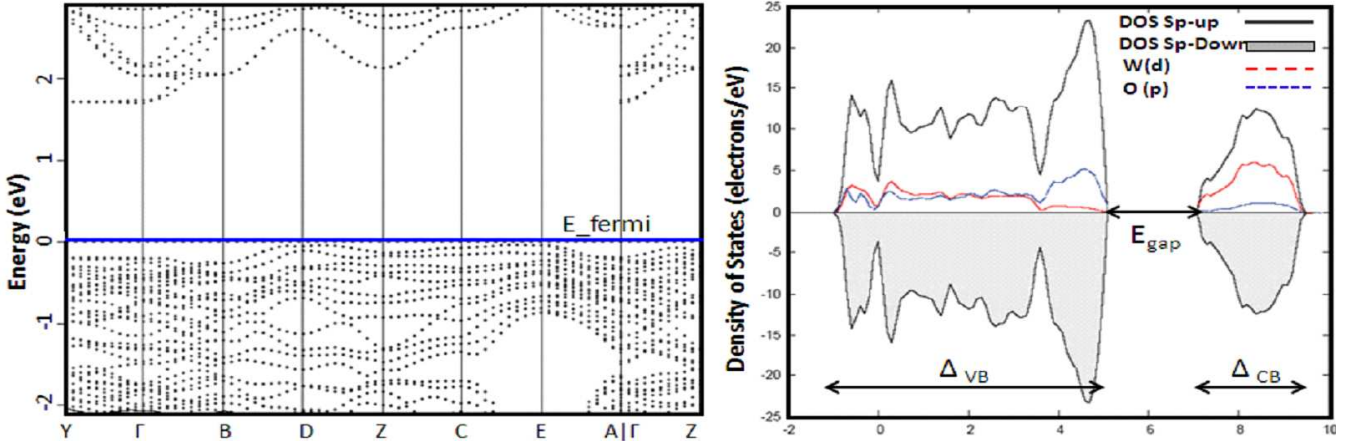


Fig. 2. BS (left) and DOS and PDOS (right) of bulk WO_3 .

In Fig. 2, we have presented the calculated BS, DOS and PDOS. The total DOS reveals that density of states for spin up and spin down are exactly the same which indicates that there is no magnetic moment for pure WO_3 . The PDOS plot depicts that the valence band (VB) mainly consists of the $2p$ states of O in range of -1.0 eV to 5.09 eV near the Fermi energy edge, and d -orbital states of W predominantly plays a main role for the conduction band (CB) above the Fermi level. One can see that in comparison with other transition metal oxides such as ZnO or TiO_2 $5d$ -orbitals in conduction band of WO_3 are more effective and this can produce a more un-

stable bounding in this material which conduce that WO_3 crystallizes in different modified structure easily [26, 27]. In order to compare the defected and doped systems with pure WO_3 , we have presented some of the calculated electronic data in Table I. It contains VB width (Δ_{VB}), CB width (Δ_{CB}), integral of DOS plot along CB and VB, band gap (E_{gap}), gap type and magnetization (μ_{tot}) of pure, defected and doped WO_3 .

3.2. Defected WO_3

Using the same supercell with 32 atoms consisting of 8 tungsten and 24 oxygen atoms, we studied the effect

of W and O vacancies separately on electronic structure of WO_3 . At the first step one of the tungsten (W) atoms was removed and the structure (W_7O_{24}) was fully relaxed

and at the next step relaxation process was repeated with removing one of the oxygen atoms (W_8O_{23}).

TABLE I

VB width (Δ_{VB}), CB width (Δ_{CB}), Integral of DOS plot along CB and VB, band gap (E_{gap}), gap type and magnetization (μ_{tot}) of defected and doped WO_3 in comparison with bulk.

System		Δ_{VB} [eV]	$\int \text{DOS}_{\text{VB}}$	Δ_{CB} [eV]	$\int \text{DOS}_{\text{CB}}$	E_{gap} [eV]	Gap type	μ_{tot} [$\mu_{\text{B}}/\text{cell}$]
Bulk	WO_3	6.1	192	2.9	38	1.89	(D) $\Gamma \rightarrow \Gamma$	0.00
W-vacancy	$\text{W}_{0.88}\text{O}_3$	6.6	138	3.8	37	0.66	(ID) $E \rightarrow B$	2.16
O-vacancy	$\text{WO}_{2.88}$	6.4	138	3.4	40	0.14	–	2.00
Pd-Doped	$\text{Pd}_{0.12}\text{W}_{0.88}\text{O}_3$	6.9	196	3.1	40	0.86	(ID) $A \rightarrow \Gamma$	2.11
	$\text{Pd}_{0.25}\text{W}_{0.75}\text{O}_3$	7.5	200	3.1	40	0.21	(ID) $B \rightarrow \Gamma$	-0.01
	$\text{Pd}_{0.37}\text{W}_{0.63}\text{O}_3$	–	204	–	39	–	no gap	0.00
	$\text{Pd}_{0.50}\text{W}_{0.50}\text{O}_3$	7.8	208	3.4	42	0.16	–	0.00
Pt-Doped	$\text{Pt}_{0.12}\text{W}_{0.88}\text{O}_3$	7.8	196	2.5	40	0.46	(ID) $A \rightarrow \Gamma$	-0.46
	$\text{Pt}_{0.25}\text{W}_{0.75}\text{O}_3$	8.2	200	2.7	40	0.37	(ID) $B \rightarrow \Gamma$	-2.51
	$\text{Pt}_{0.50}\text{W}_{0.50}\text{O}_3$	8.5	208	2.7	42	0.32	(ID) $B \rightarrow \Gamma$	-3.86
Au-doped	$\text{Au}_{0.12}\text{W}_{0.88}\text{O}_3$	7.8	197	3.1	41	0.23	(ID) $C \rightarrow \Gamma$	-1.07
	$\text{Au}_{0.25}\text{W}_{0.75}\text{O}_3$	–	202	–	40	–	no gap	0.00
	$\text{Au}_{0.37}\text{W}_{0.63}\text{O}_3$	8.0	207	2.8	43	0.11	(ID) $A \rightarrow \Gamma$	0.76
	$\text{Au}_{0.50}\text{W}_{0.50}\text{O}_3$	–	212	–	43	–	no gap	0.00

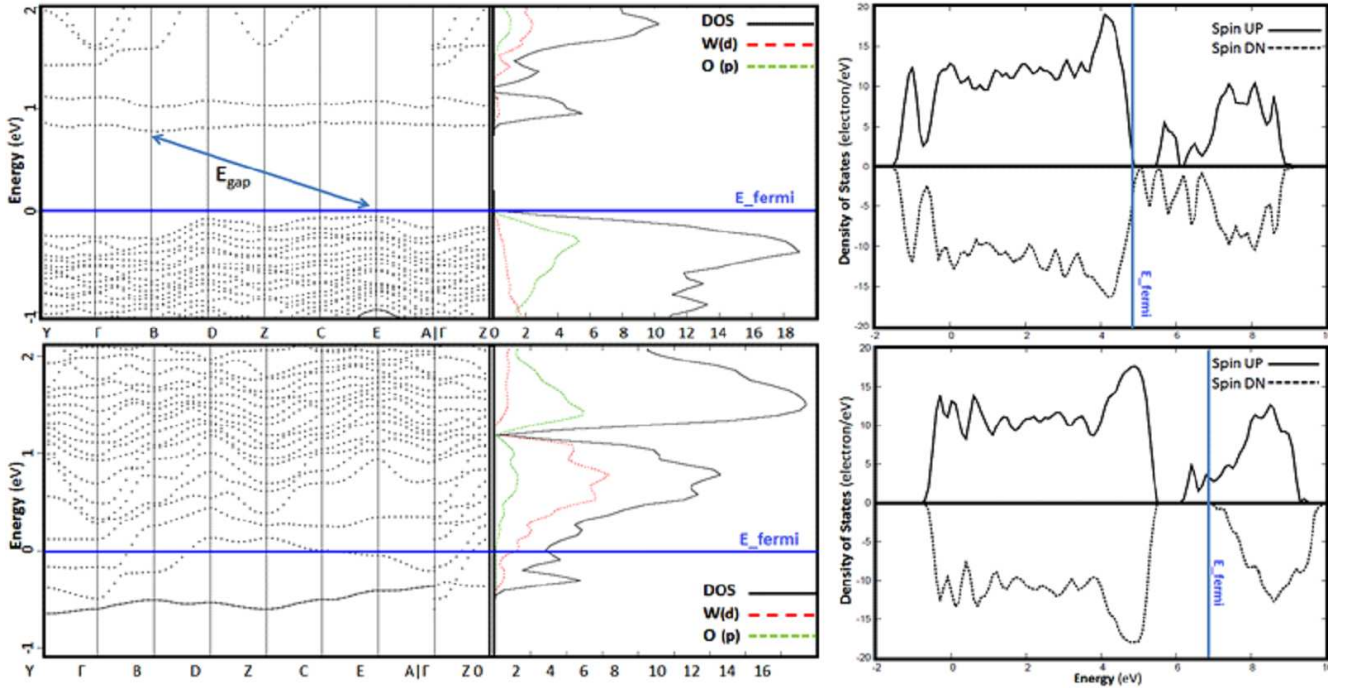


Fig. 3. BS (left) and DOS and PDOS (right) of the WO_3 with W — vacancy (top), O — (bottom).

Figure 3 presents the results of both kinds of vacancies calculations for BS, DOS and PDOS. These plots show that some new states have been generated inside the gap in both cases. In fact, W-vacancy (W_7O_{24}) ex-

hibits semiconductor state with an indirect but smaller band gap of ≈ 0.66 eV in E - B points in reciprocal lattice. In the other hand, as it is seen from BS and DOS diagrams for O-vacancy (W_8O_{23}), Fermi energy has been

shifted toward higher energies and induces a transition to metallic phase. The gap disappears completely and there is no separation between VB and CB and the density of states above E_f has been increased severely. One can notice that in spite of this fact that pure WO_3 has no magnetic moment ($\mu_{\text{tot}} = 0$), creating a vacancy of both kinds (W or O) induces magnetism in WO_3 . We obtained a total magnetization μ_{tot} of $2.16 \mu_B/\text{cell}$ for W-vacancy and $2.00 \mu_B/\text{cell}$ for O-vacancy. The above observations are in agreement with the previous works [28, 29].

3.3. Doped WO_3

At the next step we studied the effect of doping WO_3 with Pd, Pt and Au atoms. As Pt and Au belong to adjacent columns while Pd and Pt belong to two adjacent rows of periodic table, it is possible to compare the behavior of doped WO_3 versus atomic numbers and elec-

tronic shells. In order to investigate the optimized structure of $\text{A}_x\text{W}_{1-x}\text{O}_3$, we performed the relaxation calculations for Pd, Pt and Au and for four cases of $x = 0.125, 0.25, 0.375, 0.50$ (except $x = 0.575$ for Pt). In the above formula A stands for dopant. In Figs. 4–6 we present the calculated DOS, PDOS and BS plots. In the following paragraphs, at first we introduce the results for each case then analyze and compare them afterwards.

3.3.1. Pd dopant

It is seen from the BS and DOS diagrams that in $x = 0.125$, system still remains semiconductor with a smaller but indirect band gap of 0.86 eV in comparison with pure system. Meanwhile in all other amount of x , system tends to metallic phase and this behavior is improved with increasing the Pd dopant which causes a deficit of electron in this case (see Fig. 4).

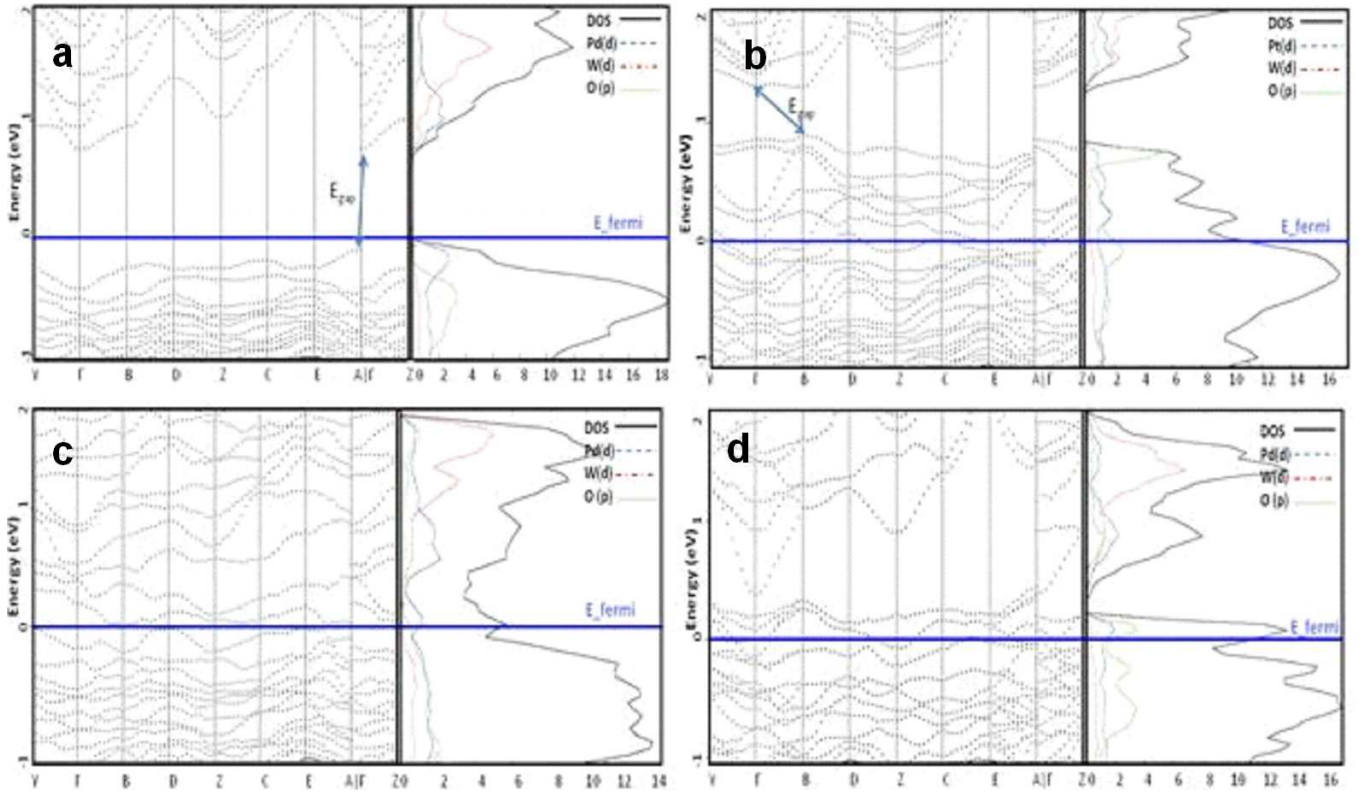


Fig. 4. BS, DOS and PDOS of $\text{Pd}_x\text{W}_{1-x}\text{O}_3$, (a) $x = 0.125$, (b) $x = 0.25$, (c) $x = 0.375$, (d) $x = 0.5$.

3.3.2. Pt dopant

BS and DOS diagrams in Fig. 5 depict that Pt impurity causes additional states inside the gap in all values of x , and thereby shifts the Fermi level into the VB, so that the systems have a transition from semiconductor to metallic phase. In addition it should be noted that W d orbital plays the main role in CB whereas there is a competition between Pd d and O p orbitals in VB. This features grow

with elevating of x value. It is also seen that gradually a wide VB is forming and electron density near the Fermi level is increasing with increase in the magnitude of Pt which can improve the electron transport properties.

Table I shows that both values of the VB width (Δ_{VB}) and the total amount of states in VB ($\int \text{DOS}_{\text{VB}}$) are increased by growing the percentage of dopant. Obviously, it should be occurred as a result of the bigger atomic

number for Pt. Although this feature is repeated for both CB width (Δ_{CB}) and the total amount of states in CB ($f \text{DOS}_{CB}$), but Δ_{CB} is less than the pure state in all cases ($2.5-2.7 < 2.9$ eV).

3.3.3. Au dopant

Results show that in WO_3 doped by Au atoms ($\text{Au}_x\text{W}_{1-x}\text{O}_3$), VB maxima and CB minima are shifted to higher energies in all cases and E_f locates inside the VB. Depending on x values, structure of band and

DOS change in an oscillatory manner (Fig. 6). As for $x = 0.25, 0.5$, VB and CB merge together and form a wide valence band. While for $x = 0.125, 0.375$ there is still a gap between CB and VB, despite that the Fermi level locates inside the VB. Regarding this matter, it is seen that in $x = 0.5$ case, system has more metallic behavior, in contrast for $x = 0.375$, the system is less metallic-like and closer to semiconducting phase.

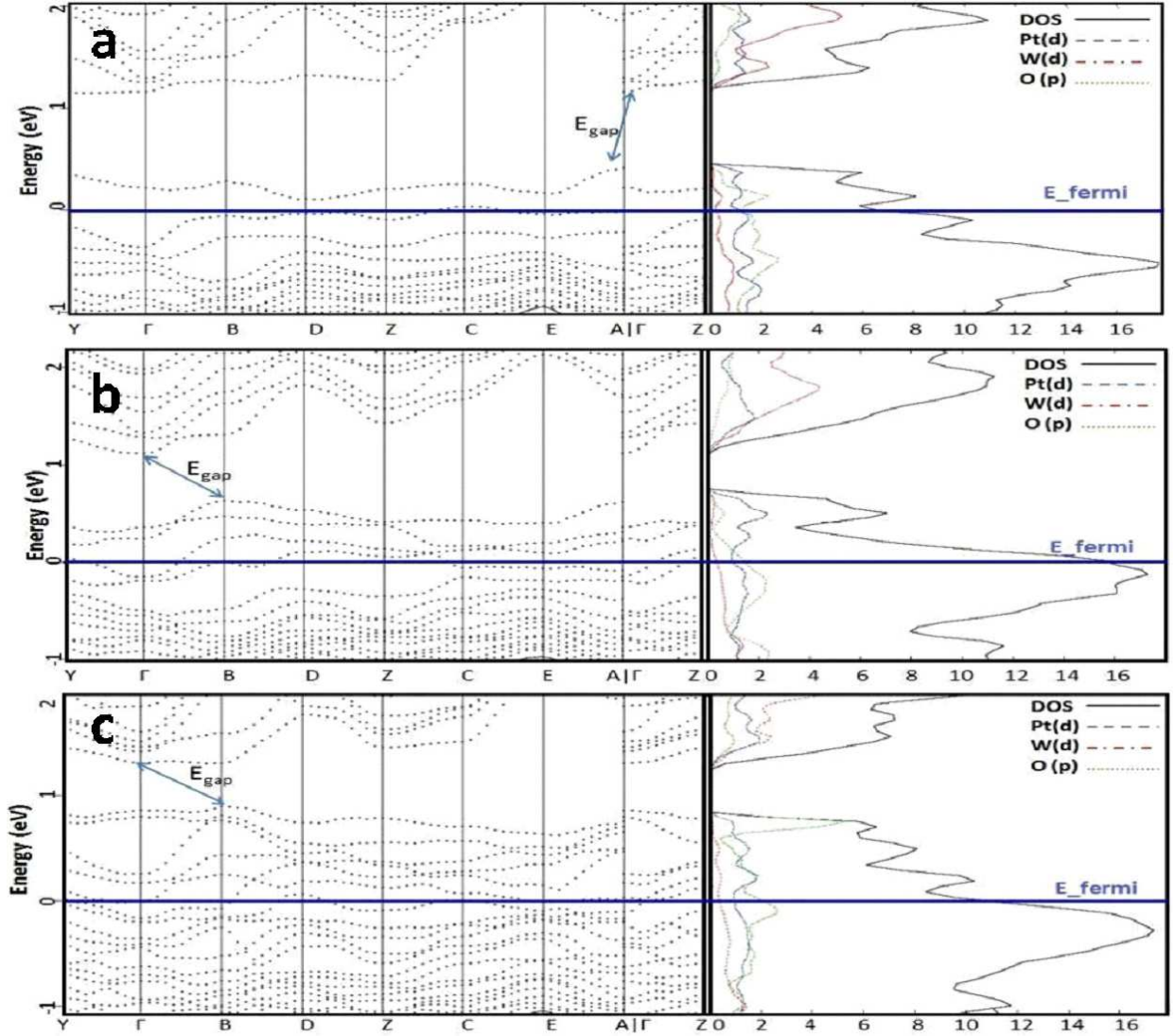


Fig. 5. BS, DOS and PDOS of $\text{Pt}_x\text{W}_{1-x}\text{O}_3$, (a) $x = 0.125$, (b) $x = 0.25$, (c) $x = 0.5$.

In brief it is seen, for all kinds of dopants, that new states start to generate inside the gap which act as trap states. With increase in the dopant atoms, the density of trap states and the width of valence and conduction band are increasing while the gap size is decreasing so that metallic behavior is improving. Moreover,

it should be noted that gap type transforms from direct for bulk system to indirect for doped systems. Besides, the gap is disappeared in $\text{Pd}_{0.375}\text{W}_{0.625}\text{O}_3$, $\text{Pd}_{0.5}\text{W}_{0.5}\text{O}_3$, $\text{Au}_{0.25}\text{W}_{0.75}\text{O}_3$, $\text{Au}_{0.5}\text{W}_{0.5}\text{O}_3$. Indeed for Au dopant, gap periodically appears and disappears as a result of shifting Au d orbital and partly O p orbital. For

$\text{Pd}_{0.5}\text{W}_{0.5}\text{O}_3$, although valence and conduction bands are almost introduced, there is no definite band gap.

Spin polarized calculations produce the possibility of magnetization calculation. Table I shows that in spite of this fact that WO_3 has not any magnetization properties ($\mu_{\text{tot}} = 0$), we find out that the Pt dopant atoms can induce magnetization for WO_3 , while Au and Pd atoms are less effective in creating magnetic properties. Actually Au and Pd atoms, just for $x = 0.125$ produce a total magnetization of $-1.07 \mu_{\text{B}}/\text{cell}$ and $2.11 \mu_{\text{B}}/\text{cell}$, respectively and in other x values we have a negligible magnetization. Increasing Pt dopant atoms increase total magnetization from -0.46 to $-3.68 \mu_{\text{B}}/\text{cell}$.

To compare the effect of dopant atom independent of the density of it, we focused the results for $x = 0.25$ of Pd, Pt and Au. As it is seen, the dopant atoms reduce the symmetry of the crystal in all of the doped systems, so that the width of both VB and CB have been increased and the d orbital of the dopant atoms has been hybridized with O $2p$ states or W d states to create new states inside

the gap. These trap states can provide electron (hole) capture or electron (hole) emission and hence improve the process of photocatalysis. For Pd and Pt, the trap states are located above the VB and not only lead to band gap narrowing but also can capture the photo-excited holes and thereby reduce the recombination rate and increase the photocurrent. In case of Pt dopant, there are additional trap states located below the CB which can act as electron capture centers. In this case, it is expected that both kinds of traps (acceptor and donor) help the optical transitions. For Au dopant, the trap states occur in the middle of the band gap and lead to active recombination center for photo-excited carriers (electron, hole) which is not suitable for the photocatalytic reactions. It is seen that enhancing the catalytic responses as a result of noble metals doping in WO_3 , can induce improving the properties such as gasochromic effect and gas sensitivity of the WO_3 based sensor. This is in agreement with the experimental results of [30–33].

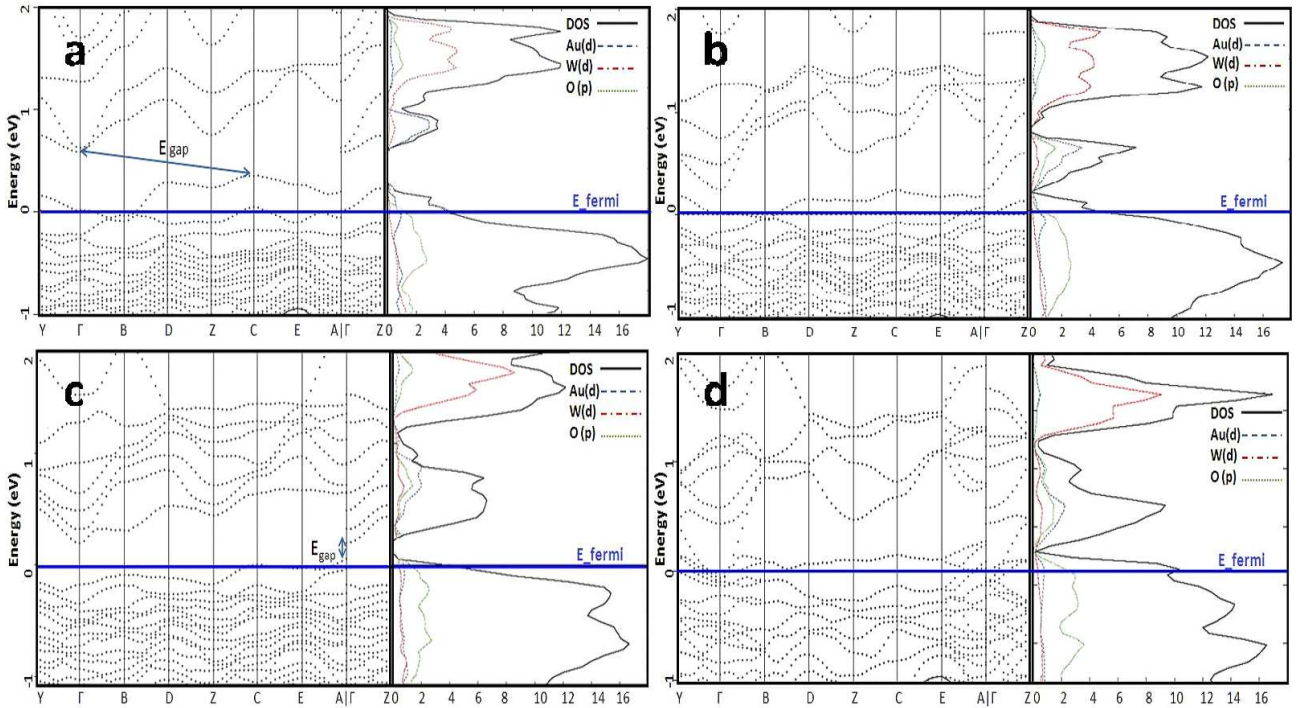


Fig. 6. BS, DOS and PDOS of $\text{Au}_x\text{W}_{1-x}\text{O}_3$, (a) $x = 0.125$, (b) $x = 0.25$, (c) $x = 0.375$, (d) $x = 0.5$.

4. Conclusion

In this paper, we have presented an overview of DFT calculation on the electronic structure and density of states for WO_3 defected with both W and O vacancies and also WO_3 doped with transition metals. These calculations show that W-vacancy remains WO_3 as a semiconductor with an indirect band gap while O-vacancy causes

a transition to metallic phase. Moreover, doping of WO_3 with transition metals illustrate that d orbitals of dopant atoms produce trap states inside the gap which affect on the electron (hole) transition rate. Indeed, palladium and platinum improve photocatalytic reactions while Au increases the recombination rate. Furthermore, vacancies and dopant atoms can induce magnetization in Pt case, while Au and Pd atoms are less effective.

References

- [1] W.J. Lee, Y.-K. Fang, J.-J. Ho, W.-T. Hsieh, S.-F. Ting, D. Huang, F.C. Ho, *J. Electron. Mater.* **29**, 183 (2000).
- [2] S. Reich, G. Leituss, Y. Tssaba, Y. Levi, A. Sharoni, O. Millo, *J. Supercond.* **13**, 855 (2000).
- [3] N. Yamazoe, G. Sakai, K. Shimano, *Catal. Surv. Asia* **7**, 63 (2003).
- [4] L. Liang, J. Zhang, Y. Zhou, J. Xie, X. Zhang, M. Guan, B. Pan, Y. Xie, *Sci. Rep.* **3**, 1936 (2013).
- [5] X.-Y. Xue, B. He, S. Yuan, L.-L. Xing, Z.-H. Chen, C.-H. Ma, *Nanotechnology* **22**, 395702 (2011).
- [6] H. Ming, W. Wei-Dan, Z. Jing, Q. Yu-Xiang, *Chin. Phys. B* **20**, 102101 (2011).
- [7] G. Korotcenkov, *Mater. Sci. Eng. B* **139**, 1 (2007).
- [8] E. Della Gaspera, A. Martucci, M. Yaacob, J. Ou, K. Kalantar-Zadeh, W. Wlodarski, *Sensor Lett.* **9**, 595 (2011).
- [9] P. González-Borrero, F. Sato, A. Medina, M. Baesso, A. Bento, G. Baldissera, C. Persson, G.A. Niklasson, C.G. Granqvist, A.F. da Silva, *Appl. Phys. Lett.* **96**, 061909 (2010).
- [10] S.Y. Chai, Y.J. Kim, W.I. Lee, *J. Electroceram.* **17**, 909 (2006).
- [11] I.R. Shein, A.L. Ivanovskii, *JETP Lett.* **95**, 66 (2012).
- [12] S. Raj, D. Hashimoto, H. Matsui, S. Souma, T. Sato, T. Takahashi, S. Ray, A. Chakraborty, D. Sarma, P. Mahadevan, W.H. McCarroll, M. Greenblatt, *Phys. Rev. B* **72**, 125125 (2005).
- [13] R. Abe, H. Takami, N. Murakami, B. Ohtani, *J. Am. Chem. Soc.* **130**, 7780 (2008).
- [14] S. Fardindoost, F. Rahimi, R. Ghasempour, *Int. J. Hydrogen En.* **35**, 854 (2010).
- [15] D. Bocharov, A. Kuzmin, J. Purans, Y. Zhukovskii, in: doref10.1117/12.8152978th *Int. Symp. Gas Flow Chemical Lasers, International Society for Optics and Photonics*, 2008, p. 71420T-T-9.
- [16] H. Ming, Z. Jie, W. Wei-Dan, Q. Yu-Xiang, *Chin. Phys. B* **20**, 082101 (2011).
- [17] D. Bullett, *J. Phys. C Solid State Phys.* **16**, 2197 (1983).
- [18] B. Loopstra, H. Rietveld, *Acta Crystallogr. B Struct. Crystallogr. Cryst. Chem.* **25**, 1420 (1969).
- [19] P. Giannozzi, S. Baroni, N. Bonini, M. Calandra, R. Car, C. Cavazzoni, D. Ceresoli, G.L. Chiarotti, M. Cococcioni, I. Dabo, *J. Phys. Condens. Matter* **21**, 395502 (2009).
- [20] S. Baroni, A. Dal Corso, S. de Gironcoli, P. Giannozzi, C. Cavazzoni, G. Ballabio, S. Scandolo, G. Chiarotti, P. Focher, A. Pasquarello, "Quantum ESPRESSO: open-source package for research in electronic structure, simulation, and optimization", code available from www.quantum-espresso.org, 2005.
- [21] W. Kohn, A.D. Becke, R.G. Parr, *J. Phys. Chem.* **100**, 12974 (1996).
- [22] J.P. Perdew, K. Burke, M. Ernzerhof, *Phys. Rev. Lett.* **77**, 3865 (1996).
- [23] A.D. Walkingshaw, N.A. Spaldin, E. Artacho, *Phys. Rev. B* **70**, 165110 (2004).
- [24] M.N. Huda, Y. Yan, S.-H. Wei, M.M. Al-Jassim, *Phys. Rev. B* **80**, 115118 (2009).
- [25] I.N. Yakovkin, M. Gutowski, *Surf. Sci.* **601**, 1481 (2007).
- [26] Y. Dong, L. Brillson, *J. Electron. Mater.* **37**, 743 (2008).
- [27] F. Tian, C. Liu, *J. Phys. Chem. B* **110**, 17866 (2006).
- [28] G. Baldissera, C. Persson, *Europ. Phys. J. B* **86**, 1 (2013).
- [29] F. Wang, C. Di Valentin, G. Pacchioni, *Phys. Rev. B* **84**, 073103 (2011).
- [30] R. Abe, H. Takami, N. Murakami, B. Ohtani, *J. Am. Chem. Soc.* **130**, 7780 (2008).
- [31] M. Penza, C. Martucci, G. Cassano, *Sensors Actuat. B* **50**, 52 (1998).
- [32] M. Zayat, R. Reisfeld, H. Minti, B. Orel, F. Sveg, *J. Sol-Gel Sci. Technol.* **11**, 161 (1998).
- [33] B. Orel, N. Gros'elj, U. Opara Kras'ovec, M. Gabrs'ek, P. Bukovec, R. Reisfeld, *Sensors Actuat. B* **50**, 234 (1998).